# Simulation of 3D Solid Tumour Angiogenesis Including Arteriole, Capillary and Venule

Jie Wu[∗,†], Quan Long[‡], Shixiong Xu[∗], Anwar R. Padhani[§] and Yuping Jiang[¶]

**Abstract:** In this paper, a 3D mathematical model of tumour angiogenesis is developed, to generate a functional tumour vasculature for blood microcirculation. The model follows that of Anderson and Chaplain (1998) [1] with three exceptions: (a) extending the model from 2D to 3D, one arteriole and one venule is induced as two parent vessels to form an intact circulation network for blood flow; (b) generating networks able to penetrate into the tumour interior rather than the exterior only; (c) considering branching generations with different diameters, based on which three groups of vessels, such as arterioles, venules and capillaries are classified. The present study contains four steps: 1. Generation of 3D angiogenic vasculature induced from one arteriole and one venule, with branching generations considered. 2. Examination of vessel connectivity among each other to construct a functional network for blood circulation, investigation of sensitivity of network architectures to changes in some model parameters. 3. Simulation of blood flow in the developed vasculatures. 4. Comparisons of blood flow calculated on the networks induced from an arteriole-venule system and from a single parent vessel.

The networks from simulations could present basic geometric and morphological features of tumour vasculatures. The sensitivity analysis indicates the controllability of the created networks, which could construct architectures of some specific geometric features to suit different types of tumours. The comparisons of blood flow mentioned above demonstrate the validity of the present vasculature, which could be served as a more realistic network structure for research of microcirculation, drug delivery in solid tumors.

## 1 Introduction

Angiogenesis is the process by which new blood vessels develop from an existing vasculature, through endothelial cell sprouting, proliferation and fusion [2]. Tumour angiogenesis plays an essential role in cancer biology. It is believed that angiogenesis will start to occur when a small avascular tumor exceeds some critical diameter (∼2 mm). Since normal tissue vasculature is no longer able to support its growth [3] and a new network of blood vessels must be developed to supply nutrients and oxygen, and to remove waste products. Once the angiogenic vasculature is established, tumour transfers from the relatively harmless avascular growth phase into the potentially fatal vascular one. As its significant roles in tumour development and metastasis, tumour angiogenesis has attracted the attention of investigators in a variety of fields, and become one of the most important areas of active research in the theoretical biology community.

Over the past 15 years or so, there has been a renewed interest in the mathematical modeling of it. The models mainly focused on the role played by endothelial cells during the formation of the new blood vessels. They can be broadly divided into two categories: (1) Continuum Models: usually derived from mass conservation equations and chemical kinetics. They result in a system of

∗ Department of Mechanics and Engineering Science, Fudan University, Shanghai, China

† Brunel Institute for Bioengineering, Brunel University, Uxbridge, Middlesex, UK

‡ Corresponding Author. Brunel Institute for Bioengineering, Brunel University, Uxbridge, Middlese, UB8 3PH, UK. Email: quan.long@brunel.ac.uk

§ Paul Strickland Scanner Centre, Mount Vernon Hospital, Northwood, Middlesex, UK

¶ Department of neurology, Huashan hospital, Fudan University, Shanghai, China

partial different equations, modeling macroscopic quantities such as cell density and chemical concentrations [4−7]; (2) Discrete Model: often contain a stochastic element and model at the level of the individual cell. They attempt to capture microscopic properties of the capillary network, such as sprout branching and looping, by keeping track of the movements of each individual cell [1,8−13]. Compared with continuum models, discrete models can be used to simulate and display the evolutionally process of tumour angiogenesis, and eventually generate a vascular network consistent with experimental observations in vivo. Most of the above models were carried on 2D domain with a single parent vessel, from which the network grows. The generated networks were confined to the regions outside the tumour, without considering the vessels growing into the tumour interior. However, in order to survive and grow, tumours need to maintain a functional vascular network, that is, the network should form an intact circulation domain for blood flow, flowing from the host arterioles, through the capillary network and collected by the venules. But in those studies, no such vasculatures had been developed.

In contrast, the main purpose of this paper is to develop a numerical method to generate 3D tumour angiogenic networks functional for blood microcirculation, to provide a relatively effective and valid vasculature model for the future study of coupled intravascular-interstitial flow and drug delivery in tumours. The present model of tumour angiogenesis follows that of Anderson and Chaplain (1998) [1] with three exceptions: (a) The original 2D model is extended into 3D, one arteriole and one venule is induced as two parent vessels in order to form a functional microcirculation vasculature; (b) The angiogenic network is simulated penetrating into the tumour interior rather than the exterior only, in consideration of the heterogeneous spatial mechanical environments of different tumour regions; (c) The branching generations with different vessel diameters are also taken into account, based on which three groups of arterioles, venules and capillaries are classified.

The study in this paper contains four steps: 1. Generation of 3D angiogenic vasculature induced

from one arteriole and one venule, with branching generations considered. 2. Examination of vessel connectivity among each other in order to construct a functional network for blood circulation, investigation of the sensitivity of the created network architectures to the changes in some model parameters. 3. Simulation of the blood flow in the developed vasculature. 4. Comparisons of the blood flow calculated on the network induced from an arteriole-venule system and from a single parent vessel, for demonstration of the validity of the present angiogenesis model.

## 2  Mathematical Models

### 2.1  3D Model of Tumour Angiogenesis

The present 3D model is inspired by the 2D tumour angiogenesis model initially proposed by Anderson and Chaplain (1998) [1]. The model assumes that endothelial cells (ECs) migrate through random motility, chemotaxis in response to tumour angiogenesis factors (TAFs) and haptotaxis in response to fibronectin (FN) gradients in the excellular matrix (ECM). We denote the EC density per unit area $n$, the TAF concentration $c$ and the FN concentration $f$, and the nondimensional equations describing the vascular growth process is given by [1]

$$\frac{\partial n}{\partial t} = \overbrace{D\nabla^2 n}^{random\,motility} \overbrace{-\nabla \cdot (\frac{\chi}{1+\alpha c}n\nabla c)}^{chemotaxis} \overbrace{-\nabla \cdot (\rho n \nabla f)}^{haptotaxis}$$

$$\frac{\partial f}{\partial t} = \overbrace{\beta n}^{production} - \overbrace{\gamma n f}^{uptake}$$

$$\frac{\partial c}{\partial t} = -\overbrace{\eta n c}^{uptake} \tag{1}$$

The coefficients $D$, $\chi$ and $\rho$ characterize the random, chemotactic and haptotactic cell migration respectively. $\beta$, $\gamma$ and $\eta$ are coefficients describing the rates of FN production, FN degradation and TAF uptake by ECs respectively.

In order to track the motion of individual endothelial cells located at the vessel sprout tips and the subsequent formation of neo-vessels, we use the

3D discretized form of the system of partial differential equations as follows, which is obtained by the standard Euler finite difference approximation:

$$n_{l,m,n}^{q+1} = n_{l,m,n}^q P_0 + n_{l+1,m,n}^q P_1 + n_{l-1,m,n}^q P_2$$
$$+ n_{l,m+1,n}^q P_3 + n_{l,m-1,n}^q P_4 + n_{l,m,n+1}^q P_5$$
$$+ n_{l,m,n-1}^q P_6 \tag{2}$$
$$f_{l,m,n}^{q+1} = f_{l,m,n}^q (1 - k\gamma n_{l,m,n}^q) + k\beta n_{l,m,n}^q$$
$$c_{l,m,n}^{q+1} = c_{l,m,n}^q (1 - k\eta n_{l,m,n}^q)$$

where $l, m, n$ specify the location on the grid and $q$ is for the time step, i.e. $x = l\Delta x$, $y = m\Delta y$, $z = n\Delta z$ and $t = q\Delta t$. The coefficients $P_0 - P_6$ incorporate the effects of random, chemotactic and haptotactic movement and depend upon the local chemical environment (FN and TAF concentrations). They relate to the likelihood of the cell remaining stationary ($P_0$), or moving along the $x(P_1)$, $-x(P_2)$, $y(P_3)$, $-y(P_4)$, $z(P_5)$, or $-z(P_6)$, see Fig.1. The full expressions of $P_0 - P_6$ are as follows, where $\Delta x = \Delta y = \Delta z = h$, $\Delta t = k$.

$$P_0 = 1 - \frac{6kD}{h^2} + \frac{k\alpha\chi}{4h^2(1+\alpha c_{l,m,n}^q)^2}$$
$$[(c_{l+1,m,n}^q - c_{l-1,m,n}^q)^2 + (c_{l,m+1,n}^q - c_{l,m-1,n}^q)^2$$
$$+ (c_{l,m,n+1}^q - c_{l,m,n-1}^q)^2]$$
$$- \frac{k\chi}{h^2(1+\alpha c_{l,m,n}^q)}(c_{l+1,m,n}^q + c_{l-1,m,n}^q + c_{l,m+1,n}^q$$
$$+ c_{l,m-1,n}^q + c_{l,m,n+1}^q + c_{l,m,n-1}^q - 6c_{l,m,n}^q)$$
$$- \frac{k\rho}{h^2}(f_{l+1,m,n}^q + f_{l-1,m,n}^q + f_{l,m+1,n}^q + f_{l,m-1,n}^q$$
$$+ f_{l,m,n+1}^q + f_{l,m,n-1}^q - 6f_{l,m,n}^q)$$
$$\tag{3}$$

$$P_1 = \frac{kD}{h^2} - \frac{k}{4h^2}\left[\frac{\chi}{(1+\alpha c_{l,m,n}^q)}(c_{l+1,m,n}^q - c_{l-1,m,n}^q)\right.$$
$$\left. + \rho(f_{l+1,m,n}^q - f_{l-1,m,n}^q)\right]$$

$$P_2 = \frac{kD}{h^2} + \frac{k}{4h^2}\left[\frac{\chi}{(1+\alpha c_{l,m,n}^q)}(c_{l+1,m,n}^q - c_{l-1,m,n}^q)\right.$$
$$\left. + \rho(f_{l+1,m,n}^q - f_{l-1,m,n}^q)\right]$$

$$P_3 = \frac{kD}{h^2} - \frac{k}{4h^2}\left[\frac{\chi}{(1+\alpha c_{l,m,n}^q)}(c_{l,m+1,n}^q - c_{l,m-1,n}^q)\right.$$
$$\left. + \rho(f_{l,m+1,n}^q - f_{l,m-1,n}^q)\right]$$

$$P_4 = \frac{kD}{h^2} + \frac{k}{4h^2}\left[\frac{\chi}{(1+\alpha c_{l,m,n}^q)}(c_{l,m+1,n}^q - c_{l,m-1,n}^q)\right.$$
$$\left. + \rho(f_{l,m+1,n}^q - f_{l,m-1,n}^q)\right]$$

$$P_5 = \frac{kD}{h^2} - \frac{k}{4h^2}\left[\frac{\chi}{(1+\alpha c_{l,m,n}^q)}(c_{l,m,n+1}^q - c_{l,m,n-1}^q)\right.$$
$$\left. + \rho(f_{l,m,n+1}^q - f_{l,m,n-1}^q)\right]$$

$$P_6 = \frac{kD}{h^2} + \frac{k}{4h^2}\left[\frac{\chi}{(1+\alpha c_{l,m,n}^q)}(c_{l,m,n+1}^q - c_{l,m,n-1}^q)\right.$$
$$\left. + \rho(f_{l,m,n+1}^q - f_{l,m,n-1}^q)\right]$$
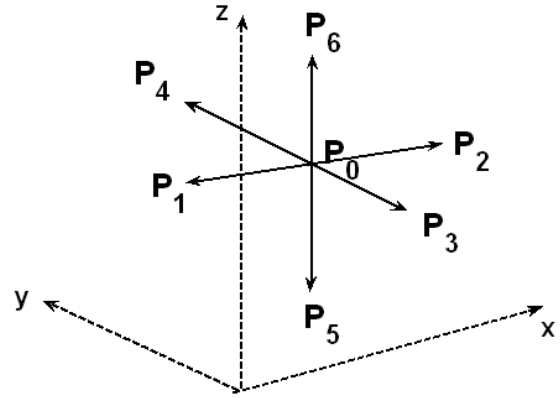


Figure 1: Motion directions of ECs in the tumour angiogenesis model.

Details of the branching rules (formation of new sprouts from existing sprout tips) and anastomoses (formation of loops by fusion of two colliding sprouts) can be found in Anderson and Chaplain (1998) [1] and Gao et al.(2005) [14]. Once the sprouts grow into the tumour, the migration will be adjusted in terms of the mechanical features of the tumour tissues [14].

A process of splitting large "mother" blood vessels into smaller "daughter" vessels, has been reported to participate in tumor vessel growth[15]. Here, we define the vessel diameter as follows,

$$d_n = g_n d_0 \quad (n = 1, 2 \ldots) \tag{4}$$

where $d_0$ is the diameter of parent vessels, $d_n$ is the diameter of the $n^{th}$ generation vessels, $g_n$ is the ratio coefficient smaller than 1. In the present model, it is assumed that, with continuously branching, the difference of the diameters between the "mother" vessels (generation $n$) and their "daughters" (generation $n+1$) decreases monotonously with $n$, accordingly $g_n$ in the above equation is prescribed by,

$$g_{n+1} = a^{\frac{1}{n+1}} g_n \tag{5}$$
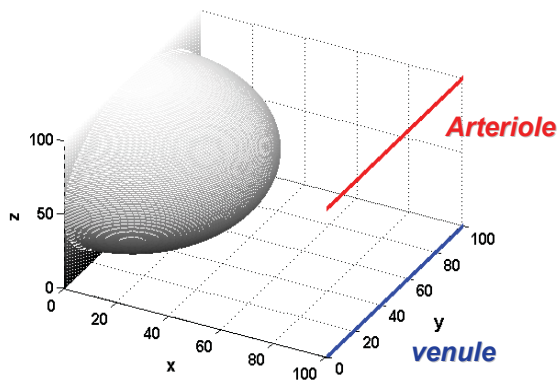
in which $a$ is a coefficient below 1.



Figure 2: Tumour angiogenesis model scheme.

The simulation is carried out on a 3D domain of 2mm×2mm×2mm, equivalent to a dimensionless domain of 1×1×1, which is divided into 100×100×100 grids with linear formulation yielding 101×101×101 nodes. The parental arteriole and venule are located on the right top and right bottom boundaries respectively, a half tumour with a radius ($R_t$) of 1 mm is on the left with a distance of $\sqrt{5}$mm from its center to each parent vessel, and surrounded by normal tissues of the host, see Fig.2. Zero flux conditions are imposed on the boundaries. The initial distribution of FN and TAF concentrations are described by

$$c(r,0) = \begin{cases} 1 & 0 \leq r \leq 0.3 \\ \frac{(v-r)^2}{v-0.4771} & 0.3 \leq r \end{cases} \tag{6}$$

$$f(r,0) = b \left( e^{-\frac{(x-1)^2+(z-1)^2}{\varepsilon}} + e^{-\frac{(x-1)^2+z^2}{\varepsilon}} \right) \tag{7}$$

where $r$ is the dimensionless distance from the tumour center and $r$=1.07, assuming the tumour has a netroic region with the radius of 0.6 $R_t$ (corresponding to $r \leq 0.3$ region). Taking Eq.(6) as the initial conditions for the TAF concentration profile might be a reasonable description of the actual concentration field arising from a circular tumor implant with a necrotic region. Parameters $b$ and $\varepsilon$ were taken to be 0.45, and 0.75 respectively, adopted from the model of Anderson and Chaplain (1998) [1].

## 2.2 3D Model of blood flow in vascular network

Flux conservation of incompressible flow was assumed at each node $c$ within the entire interconnected network [16]

$$\sum_{k=1}^{6} Q_{(c)}^k B_{(c)}^k = 0 \tag{8}$$

where the index $k$ refers to the adjacent nodes, $Q_{(c)}^k$ is the flow rate from node $k$ to node $c$, $B_{(c)}^k$ is a positive integer '1' or '0', which describes whether node $c$ and node $k$ are connecting ($B_{(c)}^k$=1) or not connecting ($B_{(c)}^k$=0) to form vascular element $k$ respectively.

$Q_{(c)}^k$ is given by the local Poiseuille expression

$$Q_{(c)}^k = \frac{\pi R_k^4}{8\mu_k} \frac{(P_{V,(k)} - P_{V,(c)})}{\Delta l_k} \tag{9}$$

where $P_{V,(c)}$, $P_{V,(k)}$ are the blood pressure of node $c$ and $k$; $\mu_k$ is the blood viscosity in vascular element $k$; $\Delta l_k$ and $R_k$ are the length and radius of the vascular element $k$.

The main purpose of the present blood flow simulation is to provide a validation of the 3D angiogenesis result rather than a comprehensive blood perfusion study. Therefore, in this study, for simplicity, the features in the microcirculation flow such as blood rheology, capillary compliance and permeability were not taken into account.
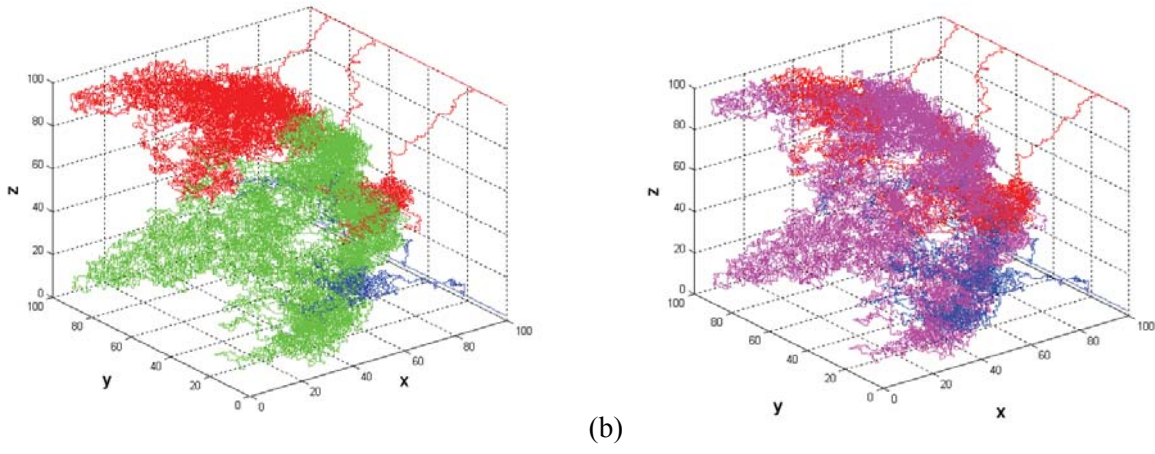
(a)                                           (b)

Figure 3: 3D angiogenic vasculature from simulation (a) The red and blue vessels represent the ones induced from the parent vessel of "arteriole" and "venule" respectively, the green ones are the "daughter" vessels after the above two kinds of vessels connected together; (b) Three groups of vessels are presented: red—arterioles, blue—venules and pink—capillaries, according to their branching generations defined in the text.

## 3   Simulation Results

### 3.1   *Angiogenic vasculature*

The values of dimensionless parameters imposed in the simulations were: $D$=0.00035, $\alpha$=0.6, $\chi$=0.38, $\rho$=0.22, $\beta$=0.05, $\gamma$=0.1, $\eta$=0.1$\varepsilon$ [1,10]. Details of the parameter normalization were given in [1]. Time was scaled as $\tilde{t} = \frac{t}{\tau}$ with $\tau = L/D_c$, where $L = 2mm$ is the length of the domain and $D_c = 2.9 \times 10^{-7} cm^2/s$ is taken as the diffusion coefficient for TAF [17,18], giving the timescale $\tau$ as about 1.5 days. The diameter of the parent vessels; $d_0$ was set as $30\mu m$, in accordance with physiological values at the microvascular scale. The baseline values of $g_1$, $a$ in Eq.(5) were given as $g_1 = 0.75$, $a$=0.65, the sensitivity analysis of the vessel diameter distribution on the change of these two parameters were presented in 'Result 3.2'. Six positions were chosen arbitrarily along the two parent vessels (three for each) as our initial sprouting sites.

Fig.3 presented the simulation results of the 3D vascular architecture. It took approximately $\tilde{t} = 14$ (corresponding to $t$=21 days) for the growth process to be completed. To check whether the vessels induced from the arteriole have interconnected with those from the venule to form an functional circulation domain for blood flow,
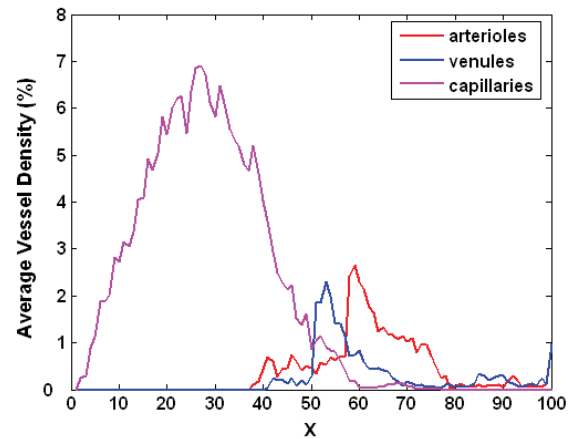


Figure 4: Distribution of the average vessel density along $x$ axis.

three colors were used to divide those vessels artificially in Fig.3(a), the red ones represented the vessels originated from the arteriole and the blue ones from the venule, once these two kind of vessels were fused together during growing, their "daughter" vessels were considered as products of the both two parent vessels and shown in green color. As for the branching generations, we defined one critical generation $n_c$ with the assumption that, if the branching generation $n$ is beyond $n_c$, the vessels (no matter induced from the ar-
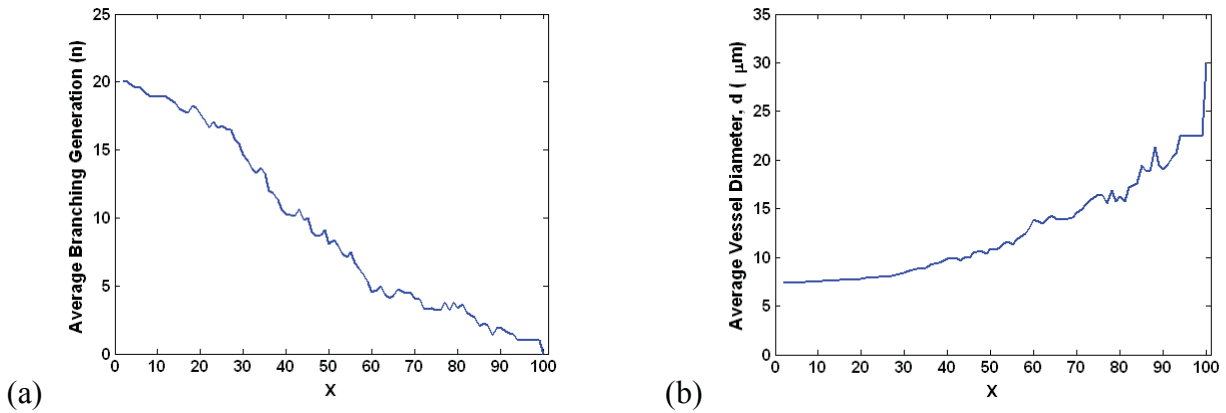
(a)                                                          (b)

Figure 5: (a) Distribution of the average branching generation along $x$ axis. (b) Distribution of the average vessel diameter along $x$ axis.



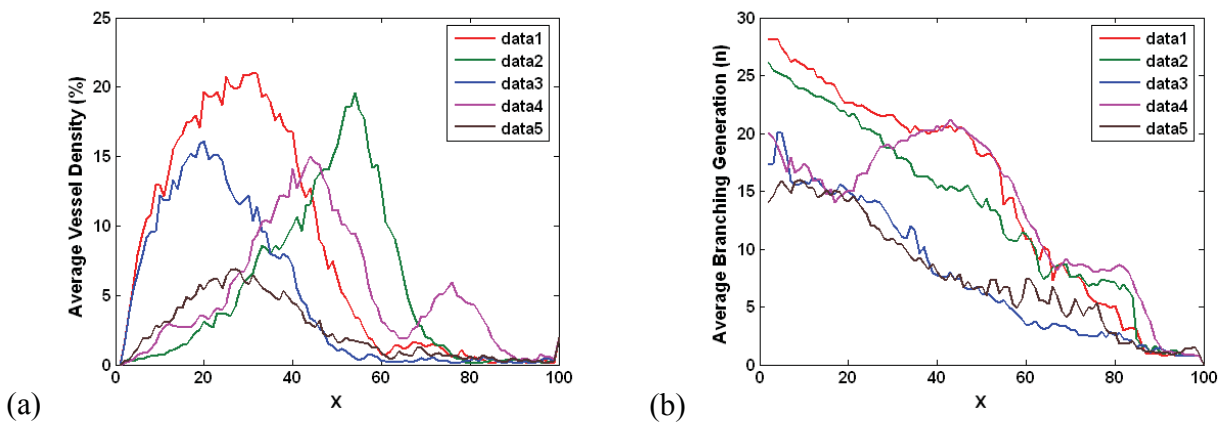(a)                                                          (b)

Figure 6: (a) Distribution of average vessel density of five vasculatures simulated with different values of $L_c$; (b) Distribution of average branching generation of five vasculatures simulated with different values of $L_c$. Data1: $L_c$=4; data2: $L_c$=5; data3: $L_c$=6; data4: $L_c$=7; data5: $L_c$=8.

teriole, the venule or both of them, as described above) were viewed as capillaries, otherwise were classified as small arterioles or venules (according to their original "mother" vessels). These three parts were presented in Fig.3(b), red—arterioles, blue—venules and pink—capillaries, here we set $n_c$=7.

From Fig.3, it shows the simulated network present the basic geometric and morphological features of tumour vasculatures, such as tortuosity, branching and anastomosis. Fig.4 is the distribution of average vessel density along $x$ axis, with three groups of vessels as arterioles, venules or capillaries. The distribution of branching generation $n$ and average vessel diameter $d$ along $x$ axis is shown in Fig.5. It indicates the vessel

branching are more easily to occur in the region of $x \in [30, 60]$, which are approximately corresponding to the well-vascularized and immediate outside area of the tumour, see in Fig.5(a), and the average vessel diameter varies slightly in the region of the tumour interior, as shown in Fig.5(b).

### 3.2 Sensitivity of vasculature geometric features

Simulations were carried out here to investigate the sensitivity of the network architectures, such as vessel density, branching generations, vascular diameter, to the changes in some model parameters. During the simulation process of angiogenesis, we adopted the branching rules as: (1) the probability for an existing sprout branching in-

creases with the local TAF concentration; (2) a sprout must reach a certain level of maturation before it becomes capable of branching. As for the second one, we defined a critical vessel length $L_c$, and vessel length $L \geq L_c$ is considered as a necessary condition for the vessel to split. In Fig.3, $L_c$ was set to be 6 (equivalent to $120\mu m$, however, due to the anastomoses in simulation, the actual shortest vessel length is smaller than $120\mu m$. According to Tozer et al.(2005) [19], average vessel length in tumours generally range from decades to hundreds). It is apparent the vascular architecture would be affected by the value of $L_c$. Fig.6(a) shows the distribution of average vessel density of five vasculatures from simulations with different values of $L_c$, they are data1: $L_c$=4; data2: $L_c$=5; data3: $L_c$=6; data4: $L_c$=7; data5: $L_c$=8. The distribution of average branching generation of these five vasculatures is given in Fig.6(b). In the present model, we also defined a relationship of branching generation $n$ with vessel diameter $d$, which is prescribed by Eq.(4) and (5). Fig.7 presents the change of average vessel diameter with parameter $a$, and different so as well (The network used is the same as Fig.3). Since for different kind or different size of tumours, the average vessel diameter would also be different. Tozer et al. (2005) [19] reported the experimental observations about the average vessel diameter with tumour diameter of some kind of tumours. In the present model, vessel diameter distribution can be adjusted easily by varying the values of above parameters in simulations. Of course, Eq.4 and 5 is just one reasonable form of controlling vessel diameter, some other forms could also be adopted. The above analysis indicate the controllability of the network structures generated from the present model, which could construct architectures of some specific geometric and morphological features to suit different types of solid tumours, by adjusting the values of related parameters.

### 3.3 Blood flow in the vasculature

In the present study, the boundary values for blood flow simulation are given by: $P_V$ =30$mmHg$ in the parent vessel of arteriole, $P_V$ =10$mmHg$ in the par-
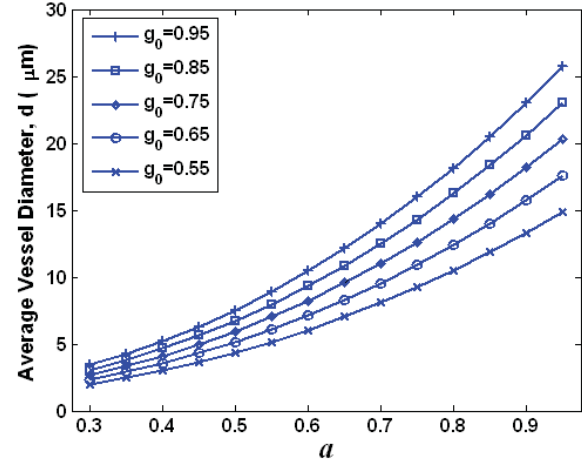


Figure 7: Relationship of average vessel diameter with parameter $a$. The network used here is the same as Fig.3.

ent vessel of venule.

Fig.8(a) and Fig.8(b) show the distribution of average blood pressure $P_V$ and blood velocity $U_V$ along $x$ axis, respectively. Three curves are presented in each figure, corresponding to the groups of arterioles, venules and capillaries defined above. According to the $P_V$ curve in Fig.8(a), it indicates that blood in the vasculature is inflowing from the parent vessel of arteriole which has the highest $P_V$, and outflowing into the parent vessel of venule possessing the lowest $P_V$ in the system. Also, it almost keeps at a constant value in the tumor interior region. As shown in Fig.8(b), blood flows much faster at the exterior and the periphery of the tumor compared with that in the interior regions. These simulation results are consistent with the experimental observations reported [19,20].

In order to demonstrate the validity of the above network with realistic arteriole-venule system, another 3D network with a single parent vessel was developed (as shown in Fig.9) and blood flow on it was calculated for comparisons. Since there is only one parent vessel to supply blood, a pressure difference of the two ends of parent vessel is required to drive blood flow. Here, the boundary values of blood pressure were given by two cases: (1) $P_{V,in}$=30$mmHg$, $P_{V,out}$=10$mmHg$; (2)

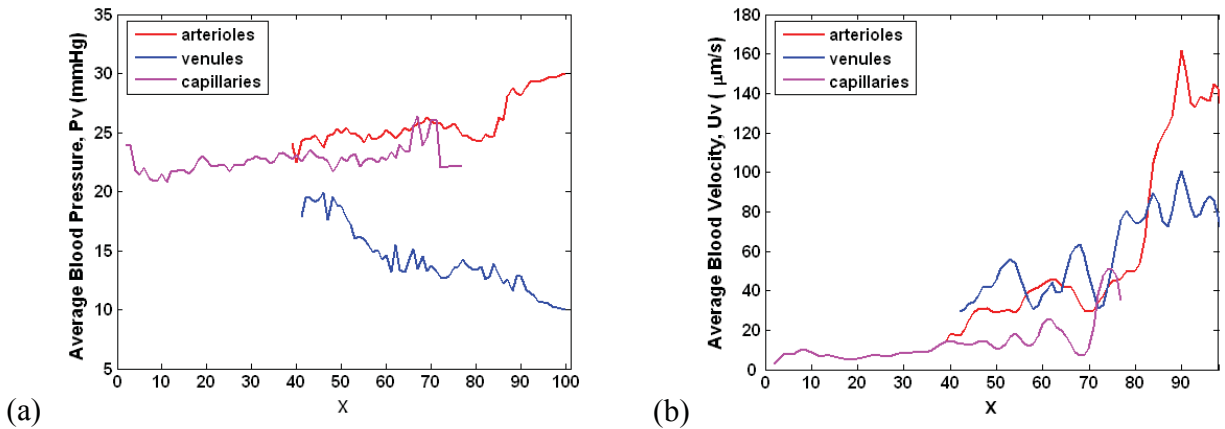(a)                                            (b)

Figure 8: (a) Distribution of the average blood pressure along $x$ axis; (b) Distribution of the average blood velocity along $x$ axis.
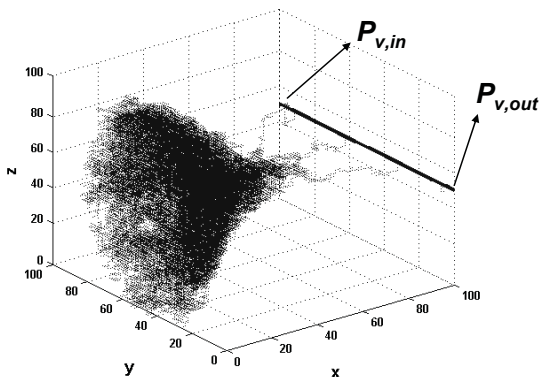


Figure 9: 3D angiogenic vasculature from simulation with one parent vessel.

$P_{V,in}$=25$mmHg$, $P_{V,out}$=18$mmHg$, see in Fig.9. The first case is chosen in accordance with the pressure difference between the arteriole and venule parent vessels in the former flow simulation, however, since the actual pressure difference along such a short vessel can not be so large, the second simulation case was also performed, whose pressure boundary values were more reasonable than that of the first one. As for Case 1, Fig.10(a) and (b) show the blood pressure distribution on $x-y$ plane of $z$=50, and the distribution of average blood pressure along $x$ axis, respectively. Compared Fig.8(a) with Fig.10(b), the average blood pressure of tumour region in Fig.8(a) is 20$mmHg$ or so, while that in Fig.10(b) is around 10$mmHg$

(approaches to the outlet pressure value), despite the same pressure difference for the parent vessel(s) from 30$mmHg$ to 10$mmHg$ were set. Generally, as a physiological value at capillary scale, average blood pressure is approximately 20mmHg, so the result presented in Fig.8(a) is more realistic. In Case 2, the pressure drop along the parent vessel was decreased. Accordingly, the average blood pressure, especially in tumour region, are enhanced with the increased outlet pressure value, see in Fig.11(a). However, the blood velocity in this case is too slow due to the small driving pressure difference in the system, as shown in Fig.11(b). In general physiological condition, intravascular blood velocity inside tumour is in the order of magnitude of 100$\mu m/s$.

## 4    Discussion

Tumor angiogenesis, the formation of a new network of blood vessels from a pre-existing vasculature, is a crucial component of solid tumor growth. Mathematical modelling of tumour angiogenesis has been a very active research area in recent years. It has largely focused on developing models to describe endothelial cell migration and proliferation through the extracellular matrix [21]. This has lead to a detailed understanding of the way in which the migration of endothelial cells is guided and governed by the gradients of angiogenic chemicals (TAFs), extra-
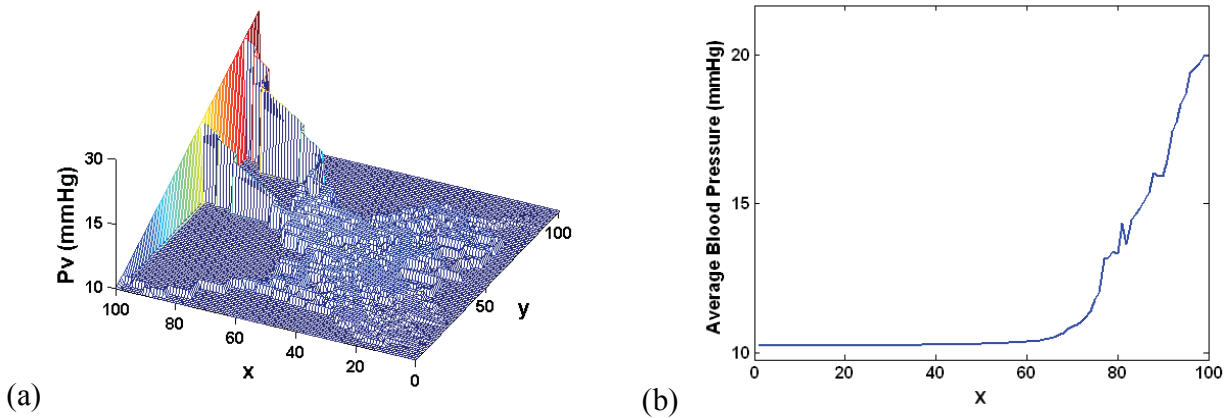
(a)



(b)

Figure 10: (a) Distribution of blood pressure in $x-y$ plane of $z$=50; (b) Distribution of average blood pressure along $x$ axis (boundary conditions of Case 1).
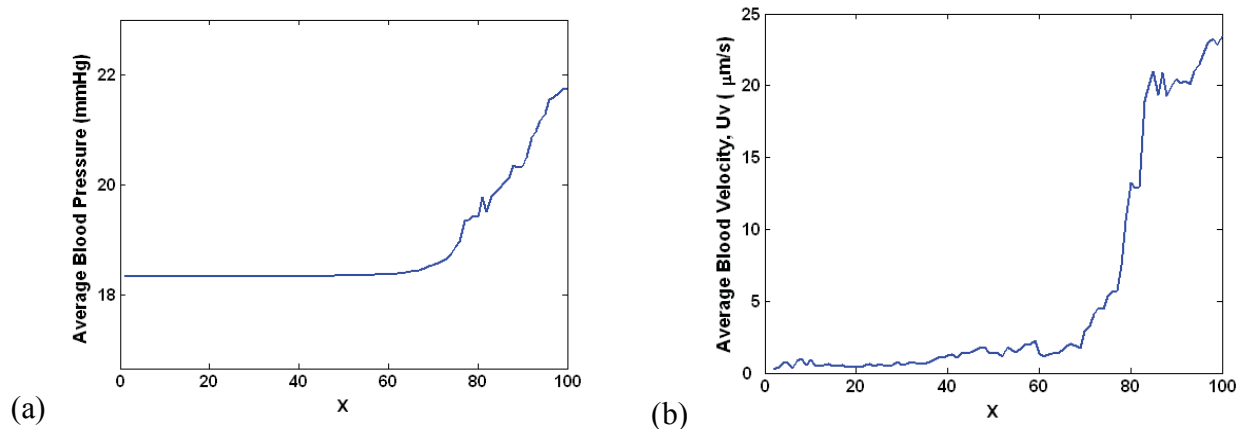


(a)



(b)

Figure 11: (a) Distribution of average blood pressure along $x$ axis; (b) Distribution of average blood velocity along $x$ axis (boundary conditions of Case 2).

cellular matrix components, and the combinations of the factors to generate the vascular networks around solid tumours. Recently, a new modeling approach—dynamic adaptive tumour-induced angiogenesis (DATIA) was described by McDougall et al., which integrates and explicitly couples a model of endothelial cell migration with a network flow model to evaluate the effects of blood perfusion and radial adaptation on a developing capillary vessel network [13].

One main purpose of modeling of tumour angiogenesis is to provide realistic network architectures of tumour microvasculature for investigation of blood perfusion or drug delivery in tumours. Therefore, an intact network with artery-vein sys-

tem for blood circulation is needed. However, the majority of previous studies only generated the networks in 2D tumour models. They were very useful on understanding the angiogenesis processes. However, the 2D network models were not suitable for blood perfusion simulation since (a) the topology could only be many unconnected region rather than a single connected region since no vessel overlap was allowed; (b) the parent vessel for supplying blood to the network had to be in the same plane. Therefore, the network cannot be separated as arteriole, capillary and venule. In contrast, the model developed in this paper aims at creating 3D tumour vasculatures to generate functional blood flow with completed arteriole-venule system. The simulation results could present the

basic geometric and morphological features of tumour vasculatures, more important, the incorporation of arteriole and venule enables the formation of a functional vasculature for blood flow, which differ radically from those generated in all previous models.

For different tumours, geometric features of their vasculatures may differ from each other greatly. Section 3.2 gave the sensitivity of some key architectural factors, such as vessel density, branching generations, vessel diameters, to the changes in the parameters of the present model. It exhibits the flexibility and controllability of network structures, and indicates that the present model could produce vasculatures of specific architectures, corresponding to not only various types of tumours, but also same tumour with different phases of its development or during the anti-angiogenesis therapy treatment.

As another novelty, classification of angiogenic vessels based on their branching generations is proposed in this paper. Three groups of vessels are defined, i.e. arterioles, venules and capillaries, see Section 3.1 for detail. The critical branching generation $n_c$, chosen as a value to divide the different groups, was also changeable if necessary. In tumour vascular systems, some vessels, such as arterioles and venules are considered as permanent components of vasculatures, whereas capillaries are often viewed as transient components. In other words, they are more likely to change, reconstruct or even disappear as the response to the environments during tumour development. Moreover, due to defective and leaky vascular basement membrane, permeability of tumour capillaries is generally much higher than that of other vessels. Therefore, we could also set different vessel permeability based on such classification, for simulations of blood perfusion in tumours, which is one of our current works.

For validation of the above work, simulations of blood flow on the angiogenic vasculatures with arteriole-venule parent vessels of the present model and with a single parent vessel as the previous models were both carried out, see in Text 3.3 by comparisons. It indicates the impact of the network structures on blood flow. Moreover, it shows that the simulation results on the arteriole-venule network are more consistent with physiological realities. It demonstrates and highlights the validity for incorporating the arteriole-veinule system into the angiogenesis model.

Allowing for the simplification of the blood flow model used in the present study, a 3D mathematical model of tumour microcirculation, which couples intravascular blood flow, transvascular leakage and interstitial fluid movement, with consideration of blood rheology and capillary compliance, is currently being developed now. It may provide an effective flow model to examine in more detail of blood perfusion in microcirculation and mass transportation in tumours and provide some new insights to therapeutic research of solid tumours.

**References**

1. Anderson, A.R.A, Chaplain, M.A.J. (1998): Continuous and Discrete Mathematical Models of Tumor-induced Angiogenesis. *Bulletin of Mathematical Biology* 60, 857-900.

2. Risau, W. (1997): Mechanisms of angiogenesis. *Nature* 386, 671-674.

3. Folkman, J. (1971): Tumor angiogenesis: therapeutic implications. *N Engl J Med.* 285: 1182-6.

4. Orme, M.E., Chaplain, M.A.J. (1996): A mathematical model of the first steps of tumour-related angiogenesis: Capillary sprout formation and secondary branching. *IMAJ. Math. Appld. Med. Biol.* 13:73-98.

5. Orme, M.E., Chaplain, M.A.J. (1997): Two dimensional models of tumour angiogenesisn and anti-angiogenesis strategies. *IMA J. of Math. Appld. Med. Biol.* 14:189-205.

6. Chaplain, M.A.J., Orme, M.E. (1998): *Mathematical modeling of tumour-induced angiogenesis*. Boston: Birkhauser. Chap. Vascular Morphogenesis: In vivo, in vitro, in mente, pp.205-240.

7. Levine, H.A., Tucker, A.L., Nilsen-hamilton, M. (2001): Mathematical modeling of the onset of capillary formaiton initiating angiogenesis. *J.Math.Biol.* 42:195-238.

8. Chaplain, M.A.J., Anderson, A.R.A. (1999): *Modeling the growth and form of capillary networks*. Chichester: Wiley. Chap. On Growth and Form: Spatio-Temporal Pattern Formation in Biology pp.225-249.

9. Chaplain, M.A.J. (2000): Mathematical modelling of angiogenesis. *J. Neuro-Oncology.* 50:37-51.

10. Stéphanou, A., McDougall, S.R., Anderson, A.R.A., Chaplain, M.A.J., Sherratt, J.A. (2005): Mathematical modeling of flow in 2D and 3D vascular networks: applications to anti-angiogenic and chemotherapeutic drug strategies, *Math. Comp. Mod.* 41, 1137-1156.

11. Stéphanou, A., McDougall, S.R., Anderson, A.R.A., Chaplain, M.A.J. (2006): Mathematical modeling of the influence of blood rheological properties upon adaptative tumour-induced angiogenesis. *Math. Comp. Mod.* 44, 96-123.

12. Zheng, X., Wise, S.M., Cristini, V. (2005): Nonlinear simulation of tumour necrosis, neo-vascularization and tissue invasion via an adaptive finite-element/level-set method. *Bulletin of Mathematical Biology* 67:211-259.

13. McDougall, S.R., Anderson, A.R.A., Chaplain, M.A.J. (2006): Mathematical modelling of dynamic adaptive tumour-induced angiogenesis: Clinical implications and therapeutic targeting strategies. *Journal of Theoretical Biology* 241:564-589.

14. Gao, H., Xu, S.X, Cai, Y., Collins, M.W. (2005): Two Dimensional Mathematical Models of Tumor induced Angiogenesis. *Chinese Quarterly of Mechanics* 26(3), 468-471.

15. Dvorak, H.F. (2002): Vascular permeability factor/vascular endothelial growth factor: a critical cytokine in tumor angiogenesis and a potential target for diagnosis and therapy. *J Clin Oncol* 20:4368-4380.

16. McDougall, S.R., Anderson, A.R.A., Chaplain, M.A.J. (2002): Mathematical Modeling of Flow through Vascular Network: Implication for Tumor-induced Angiogenesis and Chemotherapy Strategies. *Bulletin of Mathematical Biology* 64, 673-702.

17. Sherratt, J.A and Murray, J.D. (1990): *Models of epidermal wound healing*. Proc. Roy. Soe. Lond. B241, 29-36,

18. Bray, D. (1992): *Cell Movements*. Garland Publishing, New York.

19. Tozer, G.M., Ameer-Beg, S.M., Baker, J., Barber, P.R., Hill, S.A., Hodgkiss, R.J., Locke, R., Prise, V.E., Wilson, I., Vojnovic, B. (2005): Intravital imaging of tumour vascular networks using multi-photon fluorescence microscopy. *Advanced Drug Delivery Reviews* 57, 135- 152.

20. Donnelly, E.F., Geng, L., Wojcicki, W.E., Fleischer, A.C., Hallahan, D.E. (2001): Quantified Power Doppler US of Tumor Blood Flow Correlates with Microscopic Quantification of Tumor Blood Vessels. *Radiology* 219, 166-170.

21. Chaplain, M.A.J., McDougall, S.R., Anderson A.R.A. (2006): Mathematical Modeling of Tumor-Induced Angiogenesis. *Annu. Rev. Biomed. Eng.* 8:233-57.